Journal of Materials Chemistry C

ROYAL SOCIETY OF CHEMISTRY

PAPER

View Article Online
View Journal

Cite this: DOI: 10.1039/d5tc04203h

Balancing hydrophilic *vs.* hydrophobic volumes: a new approach to enhancing the ionic conductivity of amphiphilic cyclodextrins

Jayar Espejo,†[a] Carson O. Zellmann-Parrotta,†[b] Diganta Sarkar,[c] Austin Che,[a] Vladimir K. Michaelis,[c] Todd C. Sutherland,[a] Vance E. Williams*[b] and Chang-Chun Ling*[a]

Received 27th November 2025,
Accepted 30th January 2026

DOI: 10.1039/d5tc04203h

rsc.li/materials-c

We report the synthesis, mesophase characterization, and ionic conductivity of a new family of liquid crystalline materials based on amphiphilic β-cyclodextrin (β-CD) derivatives. These unique derivatives are based on a novel design to have 14 aliphatic chains of varying lengths attached to the secondary face of β-CD *via* ester linkages, and 14 *O*-monomethyl triethylene glycol units grafted onto the primary face *via* copper(I)-mediated azide–alkyne cycloaddition (CuAAC) with the help of chlorohydrin chemistry. Compared to previously reported analogues, these amphiphilic CDs exhibit a distinct molecular geometry with an expanded hydrophilic domain. Mesophase studies reveal that derivatives bearing longer aliphatic chains (≥C10) self-assemble into thermotropic liquid crystalline phases, predominantly forming smectic A (SmA) mesophases through nanophase segregation of polar and non-polar regions, while one derivative also demonstrates the ability to form a bicontinuous cubic phase that coexists with the lamellar phase. Solid-state nuclear magnetic resonance (NMR) and variable-temperature X-ray diffraction (XRD) studies confirm the presence of long-range molecular order within the SmA phases. Moreover, impedance spectroscopy reveals that these materials exhibit excellent lithium-ion conductivity, achieving a maximum of 4.86×10^{-3} S cm^{-1}, suggesting their potential as a group of promising electrolytes based biodegradable scaffolds. This work underscores the potential of applying innovative molecular designs to enhance the performance of organic electrolytes.

A Introduction

Amphiphilic cyclodextrins (CDs) have increasingly gained interest over years for their applications in the pharmaceutical industry[1–3] and for gene delivery,[4–7] and, more recently, they have been studied for their ability to form a variety of different liquid crystal (LCs) mesophases.[8–15] These materials have shown potential utility for lithium[16–19] and proton[20] conductivity, by taking advantage of the long range order present in the mesophases. The phase behaviour of amphiphilic CDs has important implications for ion conductivity. Columnar phases are generally limited to pseudo-1D transport, whereas lamellar mesophases, with their potential for 2D charge transport, offer enhanced conductivity.

A unique advantage of CD scaffolds is their face-to-face pseudosymmetry, which separates primary hydroxyl and secondary hydroxyl groups on opposite rims of a truncated cone. For example, in β-CD **1** (Fig. 1), 14 polar oligoethylene glycol chains were placed at the secondary face and nonpolar 7 *n*-octadecyl chains were installed at the primary face, generating amphiphilic CDs that formed smectic mesophases. Inverting the geometry by placing 7 oligoethylene glycol chains at the primary face and 14 *n*-octadecanoyl chains at the secondary face led to the formation of columnar hexagonal mesophases (compound **2**, Fig. 1). Similar to the phase behaviour of amphiphilic diblock copolymers,[21,22] self-assembly of amphiphilic CDs is governed by the relative volumes of the two components. In **1**, the volume fractions of the hydrophilic and hydrophobic regions are roughly equal, leading to lamellar (smectic) packing, whereas the hydrophobic volume fraction in **2** is much larger than the hydrophilic region, resulting in columnar hexagonal packing. Further alteration of the relative volume fractions of the polar and non-polar regions can promote 3D bicontinuous cubic (Cub_{bi}) mesophases, which exist at intermediate volume fractions between the columnar and lamellar zones of stability.

[a] *Department of Chemistry, University of Calgary, Calgary, Alberta, T2N 1N4, Canada. E-mail: ccling@ucalgary.ca; Fax: 403-289-9488; Tel: +403-220-2768*
[b] *Department of Chemistry, Simon Fraser University, Burnaby, British Columbia, V5A 1S6, Canada. E-mail: vancew@sfu.ca; Fax: +778-782-3765; Tel: +778-782-8059*
[c] *Department of Chemistry, University of Alberta, Edmonton, Alberta, T6G 2G2, Canada*
† Equal contributions.

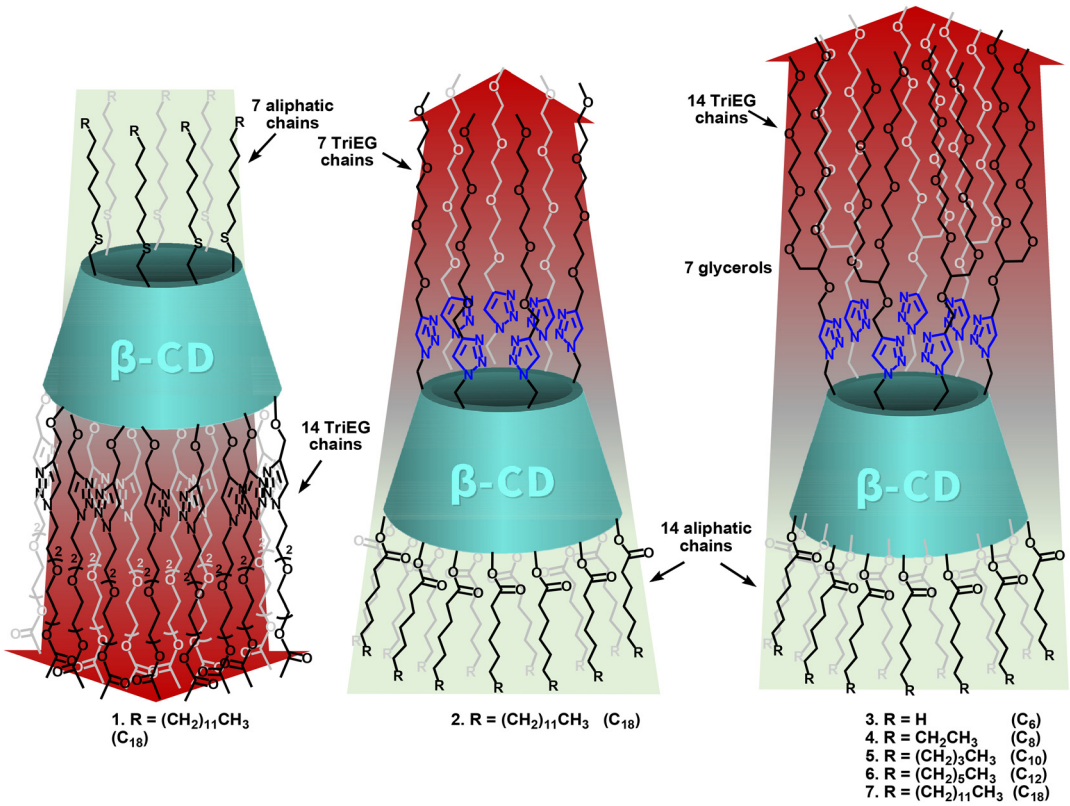

Fig. 1 Structures of previously synthesized amphiphilic β-CD derivatives capable of forming difference LC mesophases with either a 1 : 2 (**1**, smectic) or 2 : 1 (**2**, hexagonal columnar) hydrophobic/hydrophilic group ratios, and newly designed amphiphilic β-CD derivatives containing a 1 : 1 hydrophobic/hydrophilic group ratios (**3–7**); with all derivatives having 14 hydrophilic *O*-monomethyl triethylene glycol (TriEG) groups on the primary face and 14 hydrophobic acyl chains of various lengths (**3**, C_6; **4**, C_8; **5**, C_{10}; **6**, C_{12}; **7**, C_{18}) at the secondary face.

In this study, we report a new family of β-CD derivatives **3–7** (Fig. 1) decorated with 14 aliphatic esters of varying lengths at the secondary face, similar to compound **2**, but with seven branched chains on the primary face. This branching effectively doubles the number of polar *O*-monomethylated triethylene glycol chains at the primary face. The reported compounds have their secondary face esterified with 14 *n*-hexanoyl (**3**, C_6), *n*-octanoyl (**4**, C_8), *n*-decanoyl (**5**, C_{10}), *n*-dodecanoyl (**6**, C_{12}) and *n*-octadecanoyl (**7**, C_{18}) chains. By doubling the number of OEG chains at the primary face, the relative volumes of the hydrophilic and hydrophobic segments should be more equal, which we anticipate will shift LC self-assembly towards lamellar and 3D bicontinuous cubic (Cub_{bi}) mesophases compared to the parent (**2**), which forms a columnar phase. Additional OEG chains in these compounds will result in a higher hydrophilic volume which may be advantageous for ionic conduction, as these metal chelating groups provide better ionic diffusion.

B Results and discussion

Synthesis and characterization

The five newly synthesized β-CD-based liquid crystalline products **3–7** were prepared according to Scheme 1. To double the number of polar *O*-monomethyl triethylene glycol groups to the primary face, we took advantage of the epichlorohydrin chemistry.[23] Thus, the readily available *O*-monomethyl triethylene glycol (**8**), used as neat, was first deprotonated using NaH (2.1 eq.), and the resulting mixture was subsequently reacted with epichlorohydrin (**9**, 1.0 eq.) at ambient temperature followed by heating the reaction mixture to 100 °C overnight. This allowed the formation of the desired compound (**10**) which was isolated in 32% yield by column chromatography on silica gel. The identity of compound **10** was confirmed *via* NMR spectroscopy. For example, in the ^{1}H NMR spectrum, a singlet was observed at 3.33 ppm which was integrated with 6 protons; this was assigned to the two methyl groups, supporting the presence of two *O*-monomethyl triethylene glycol chains; the 2° hydrogen of the formed glycerol scaffold was observed at 3.92 ppm as a pentet (see the SI for NMR spectra).

Compound **10** was then *O*-alkylated with a propargyl group by first carrying out deprotonation with NaH (2.0 eq.) and subsequently reacting with propargyl bromide (2.0 eq.) using THF as a solvent. Compound **11** was isolated in 68% yield by column chromatography on silica gel. The presence of an *O*-propargyl group was confirmed by the presence of a doublet at 4.31 ppm (J = 2.4 Hz), and a triplet at 2.40 ppm (J = 2.4 Hz), corresponding to the methylene and alkynic protons of the propargyl group, respectively.

To introduce 14 straight aliphatic chains of various lengths (C_6, C_8, C_{10}, C_{12} and C_{18}) to the secondary face of per-6-azido-6-deoxy-β-CD (**12**),[24] we prepared anhydrides **13–17** from their

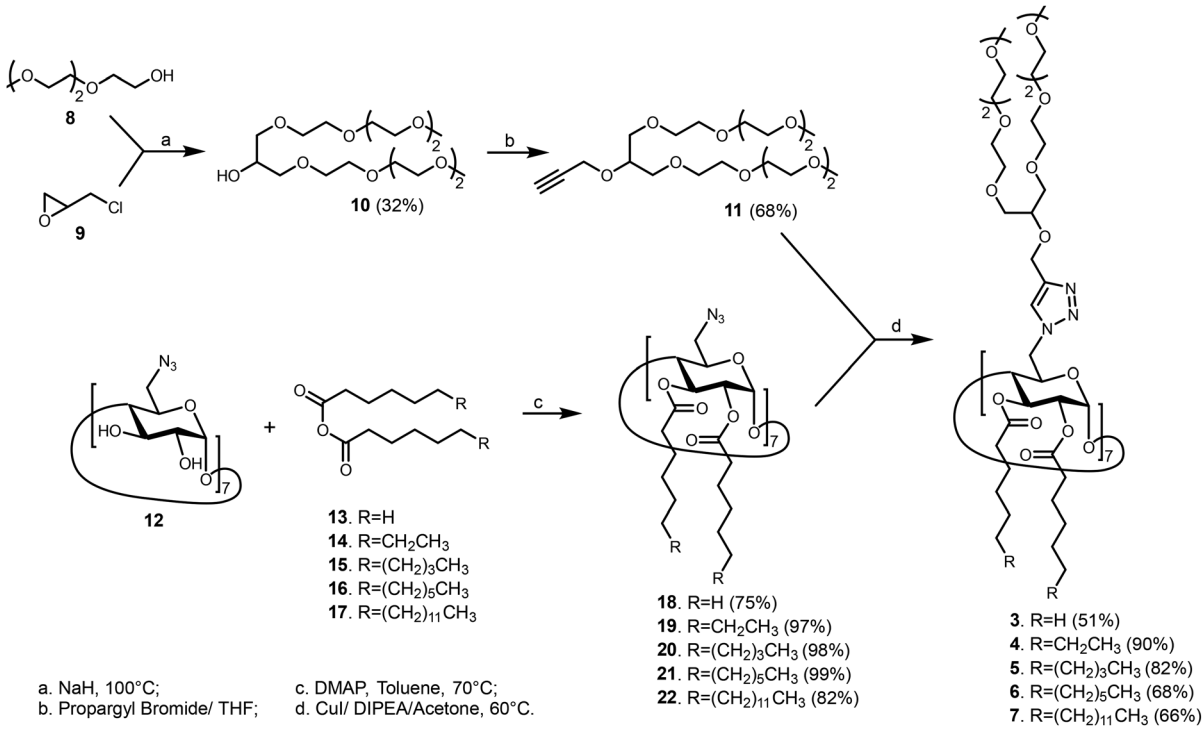

Scheme 1 Synthetic scheme of amphiphilic β-CD derivatives **3–7**.

respective aliphatic acids using *N*,*N*-dicyclohexylcarbodiimide (DCC) as the dehydrating reagent, and reacted the respective crude anhydride with compound **12** in anhydrous toluene, using 4-*N*,*N*-dimethylaminopyridine as a base at 70 °C; this afforded desired per-2,3-*O*-esterified β-CD intermediates **18–22** in good to excellent yields (75–99% yields).

With all compounds **18–22** in hand, the final conjugation step was to react with the 1,3-bis(*O*-monomethyl triethylene glycol)-2-*O*-propargyl-substituted glycerol **11** *via* "click" chemistry.[25] This reaction utilizes the copper(I) iodide as a catalyst in the presence of *N*,*N*-diisopropylethylamine (DIPEA) as a base and was carried out in acetone at 50 °C; the alkyne **11** was used in excess (2.0 equiv. per azide). After heating for 4 days, the desired conjugates **3–7** were obtained. The copper salts were effectively removed by extraction (x2) during workup using saturated aqueous EDTA solutions. Compound **3** (C_6) was purified *via* precipitation of the reaction mixture in a mixture of toluene–hexane (1 : 9,) and isolated in 51% yield. In a similar manner, compound **4** (C_8) was isolated in 90% yield *via* precipitation in a mixture of methanol–water (2 : 8). The other three final targets **5** (C_{10}), **6** (C_{12}) and **7** (C_{18}) were also isolated in a similar manner in 82%, 68%, and 66% yields, respectively.

The structures of the five targeted β-CD derivatives **3–7** were characterized *via* 1D ^{1}H and ^{13}C, 2D ^{1}H–^{1}H gCOSY, and ^{1}H–^{13}C gHSQC NMR experiments. For example, for compound **7** (C_{18}), a singlet at 7.78 ppm was observed, which was assigned to the seven 1,2,3-triazole protons. Another broad peak at 5.50 ppm and a broad doublet of doublet (J = 8.9, 8.9 Hz) at 5.40 ppm were also observed, and they were assigned to the seven anomeric protons H-1's and the seven H-3's of the glucopyranosyl units. The successful syntheses of compounds **3–7** were ultimately confirmed using mass spectrometry. For example, for compound **3** (C_6), high resolution electrospray mass experiment showed a triply charged peak at m/z 1902.3847 which correlates well with the expected molecular formula $[C_{266}H_{469}N_{21}O_{105} + 3Na]^{3+}$ (calculated m/z: 1902.3894). Additionally, all mass spectra showed the absence of adducts with copper salts, confirming the effective removal of copper salts upon washing with EDTA.

Self-assembly

According to the phase diagrams of amphiphilic diblock copolymers, estimated by self-consistent mean-field theory, the lamellar phase will be favoured when the volume fractions of the hydrophilic and hydrophobic segments are similar in value (~0.35 to 0.65), while columnar organization is favoured when one segment has a much larger volume fraction.[26,27] As alluded to in the Introduction, the branched OEG chains in compounds **3–7** will raise the hydrophilic volume fraction compared to compound **2** that has a 2 : 1 ratio of *n*-octadecanoyl/*O*-triethylene glycol chains and forms a columnar hexagonal mesophase. We estimated the volume fractions of the CD derivatives **2–7** (Table 1) using group additivities,[28] an approach that we have used previously to calculate volume fractions of CD derivatives.[18] While the hydrophilic volume fraction, f, of compound **2** is ~0.26,[29] the value increases to ~0.38 for **7** (C_{18}), and increases further as the hydrophobic chains are truncated: ~0.49 for **6** (C_{12}), ~0.54 for **5** (C_{10}), ~0.60 for **4** (C_8) and ~0.67 for **3** (C_6). Hence, we anticipated that all five

Table 1 Molar volumes of hydrophobic and hydrophilic chains for reported CD derivatives. Volumes are calculated using functional group volumes[28]

Compound	$V_{hydrophobic}$ [a] (cm^3 mol^{-1})	$V_{hydrophilic}$ [b] (cm^3 mol^{-1})	f
2 (C_{18})	2483	870	0.26
3 (C_6)	764	1547	0.67
4 (C_6)	1051	1547	0.60
5 (C_{10})	1337	1547	0.54
6 (C_{12})	1624	1547	0.49
7 (C_{18})	2483	1547	0.38

[a] Volume of 14-$(CH_2)_nCH_3$ chains, where n = 17, 11, 9, 7, or 5. [b] Volume of 7-CH_2(–$OCH_2CH_2)_4$–OCH_3 chains (compound **2**) or 7-CH_2OCH–(CH_2(–$OCH_2CH_2)_3$–$OCH_3)_2$ chains for compounds **3–7**; $f = V_{hydrophilic}/(V_{hydrophilic} + V_{hydrophobic})$.

derivatives will prefer lamellar phases, with the two end members of the series, **7** (C_{18}) and **3** (C_6), potentially forming bicontinuous cubic phases, since the narrow cubic region tends to exist at hydrophilic volume fractions of ~0.35 and ~0.65 based on the phase diagrams of diblock co-polymers.[26,27]

The phase behaviour of the CD derivatives was analyzed by differential scanning calorimetry (DSC), polarized optical microscopy (POM), and X-ray diffraction (XRD). Compound **7** (C_{18}) exhibits two peaks on heating: a large enthalpy peak followed by a small enthalpy peak, which are ascribed to the solid-to-liquid crystal (LC) and LC-to-isotropic liquid (Iso) transitions, respectively. The two peaks are reproduced in the cooling run and in subsequent DSC experiments (see Fig. S39).

Slow cooling of the sample from the isotropic melt reveals birefringent fan-shaped textures under POM (Fig. 2a). The textures shear under mechanical stress, confirming the fluidity and thus the formation of a liquid crystal phase. The LC phase was further examined *via* XRD, which exhibits 3 peaks of decreasing intensity with a *d*-spacing ratio of 1 : 2 : 3. This spectrum is indexed to a lamellar phase, with the peaks corresponding to the d_{001}, d_{002}, and d_{003} planes (Fig. 3a and b). The appearance of dark domains by POM (Fig. 2a) suggests that the phase is a smectic A (SmA) phase. The layer spacing, obtained from the *d*-spacing of the 001 peak, is 56.8 Å. To determine the molecular length, we built a molecular model of compound **7**, and carried out geometry optimization using the PM3 semi-empirical method. The calculated molecular length of compound **7** is approximately 48.2 Å (Fig. 4). Because the molecules are amphiphiles, they likely adopt a SmA bilayer structure with a layer spacing that is approximately twice this molecular length. The observed layer spacing (56.8 Å) is considerably smaller, suggesting that the chains are highly interdigitated.

As compound **7** (C_{18}) is cooled, textures under POM become increasingly birefringent and lose fluidity (Fig. 2b), indicating the formation of a solid phase. The large enthalpy of the low temperature transition observed by DSC also supports formation of a solid (Fig. S39). Room temperature XRD experiments show retention of lamellar ordering, but with additional long-range order, evidenced by the appearance of an additional peak (d_{004}) at low angles and a sharp peak (likely the packing of the OEG chains) at high angles (Fig. 3c and d). We conclude that the room temperature phase is a solid smectic phase; we have previously observed this type of behaviour for other CD derivatives, including compound **2** (C_{18}), which shows retention of the columnar hexagonal structure in the solid phase.[29]

Both **6** (C_{12}) and **5** (C_{10}) display a single reversible transition using DSC with a smaller enthalpy change (Fig. S41 and S42). Slow cooling from the isotropic phase reveals streak-like textures *via* POM that are both fluid and birefringent, suggesting both form liquid crystal phases (Fig. 5 and Fig. S46 and S47). Unlike compound **7** (C_{18}), both **6** (C_{12}) and **5** (C_{10}) retain liquid crystallinity down to room temperature. XRD experiments on samples of compound **5** show similar patterns to the SmA phase of compound **7**, displaying one sharp peak (d_{001}) followed by a second peak of smaller intensity at half the *d*-spacing (d_{002}) (Fig. S50). The appearance of dark domains by POM suggests the formation of a SmA phase.

Compound **6** (C_{12}) forms a lamellar phase, as XRD experiments show peaks corresponding to the d_{001} and d_{002} planes. Additional peaks were also observed, indicating the coexistence of a second phase (Fig. 6). These peaks were indexed to those of a Cub_{bi} phase (d_{220}, d_{420}, and d_{332}), and are consistent with the diffraction pattern for the Cub_{bi} of a previously reported CD derivative (Fig. S51).[18] This biphasic behaviour, with the coexistence of both the SmA and Cub_{bi} phases, has been observed in both amphiphilic lyotropic[31,32] and thermotropic liquid crystals.[33]

The final two derivatives, **3** (C_6) and **4** (C_8), are isotropic liquids at room temperature, as POM experiments do not show

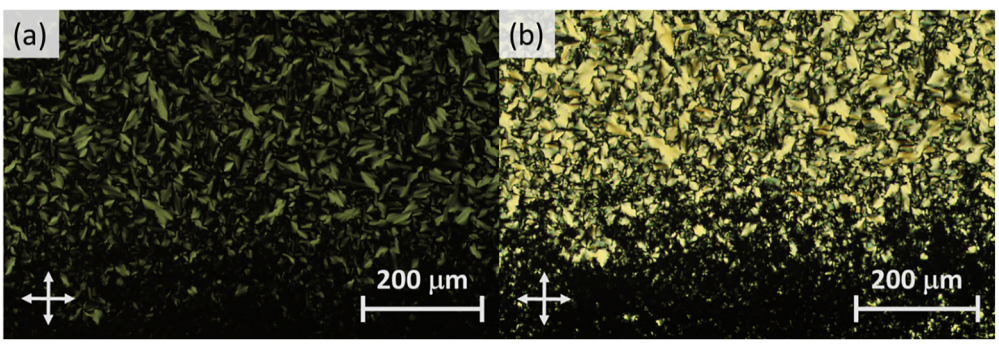

Fig. 2 Polarized optical micrographs of **7** (C_{18}) at (a) 83 °C and (b) room temperature.

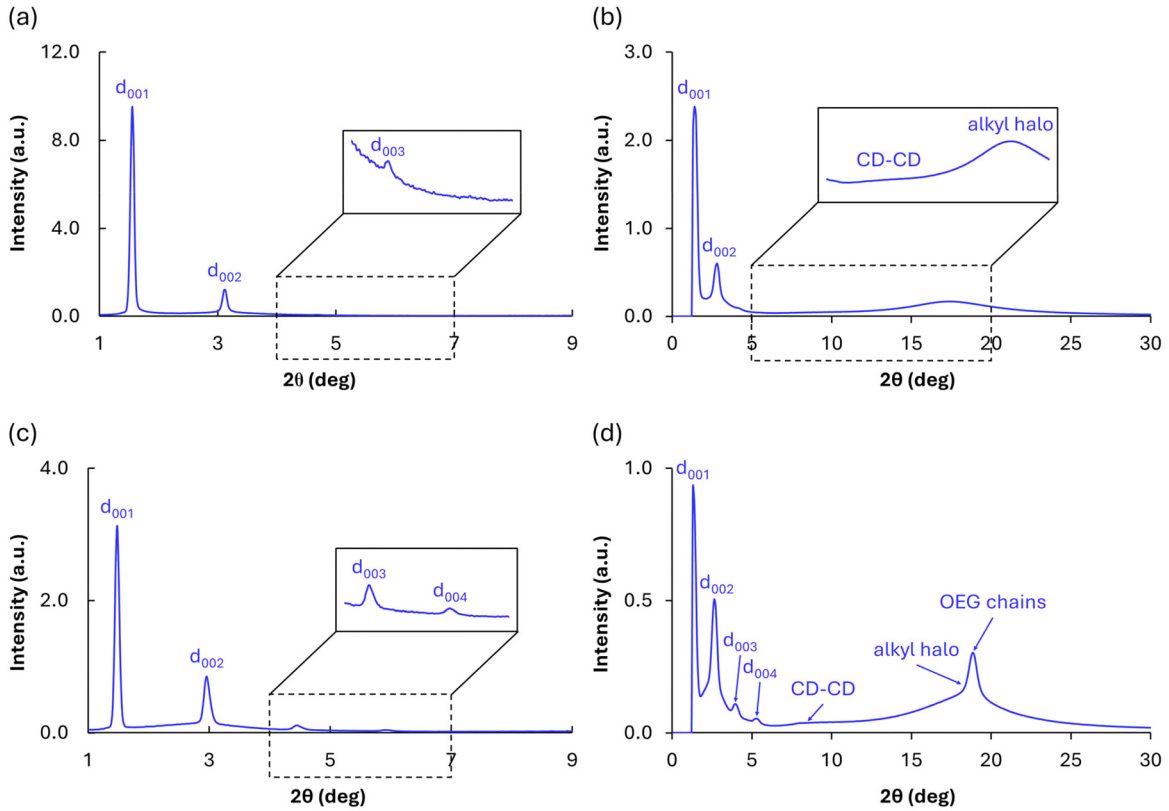

Fig. 3 X-ray diffractograms of **7** (C18) at (a) and (b) 70 °C and (c) and (d) 25 °C, showing the mid-angle scattering (left) and wide-angle scattering (right) measurements.

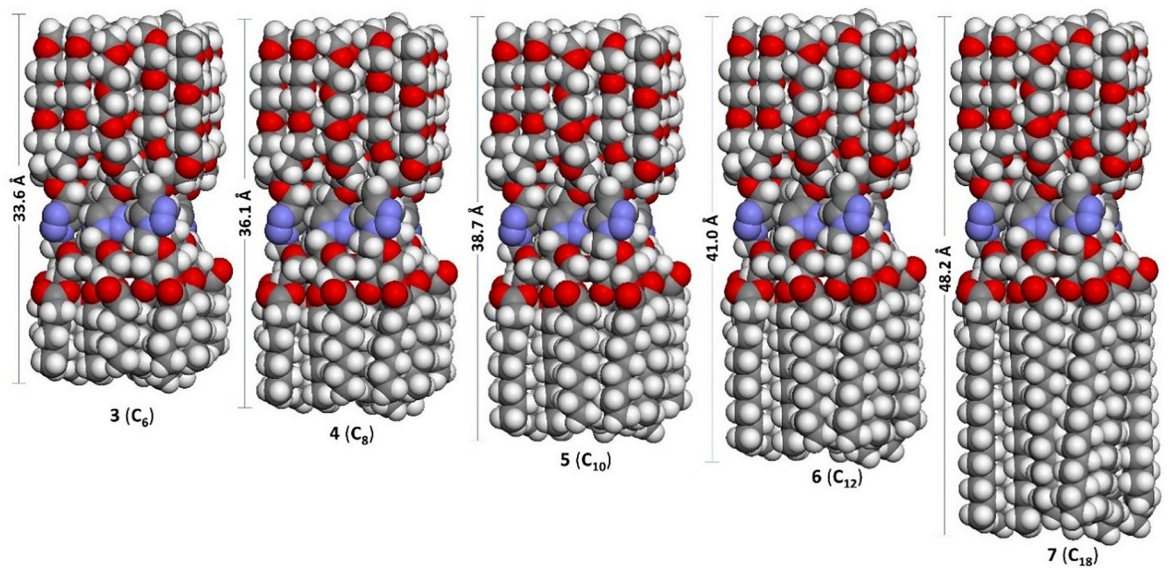

Fig. 4 CPK models and their approximate molecular lengths of synthesized amphiphilic β-CD derivatives **3–7** based on the optimized structures *via* the PM3 semi-empirical method provided using the Orca Quantum Chemistry package (Version 5.0.4).[30]

birefringence, and XRD experiments only show weak and broad peaks, consistent with isotropic liquids (Fig. S53 and S54). No transitions are observed *via* DSC between 0 and 100 °C (Fig. S43 and S44), confirming the isotropic nature of both compounds **3** and **4**. The phase behaviour of all five derivatives is summarized in Table 2.

Lamellar phases were anticipated for compounds **5**, **6** and **7** based on their *f* values (0.38, 0.49 and 0.54, respectively). The

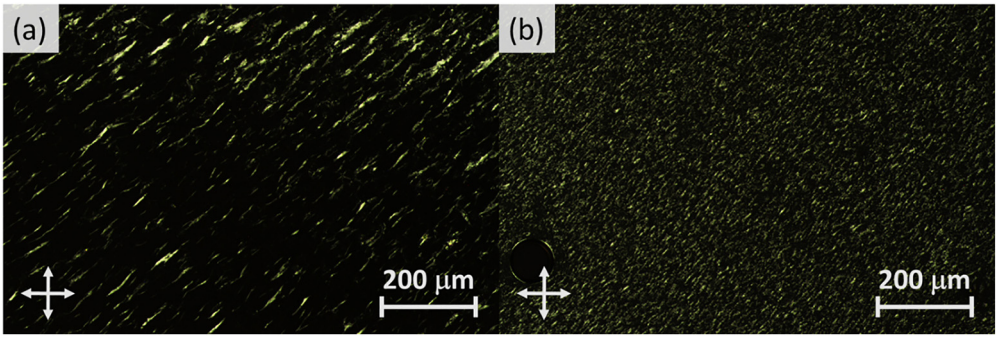

Fig. 5 Polarized optical micrographs of (a) **6** (C_{12}) at 48 °C and (b) **5** (C_{10}) at 36 °C.

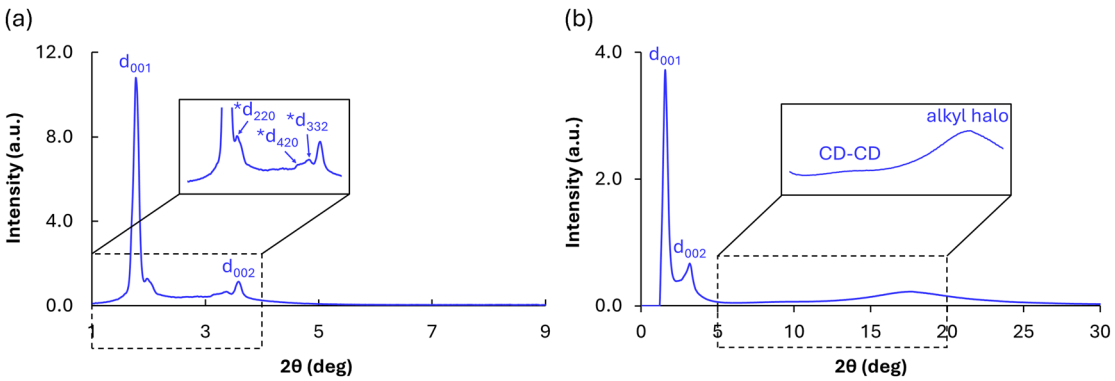

Fig. 6 X-ray diffractogram of **6** (C_{12}) at 55 °C showing the (a) mid-angle scattering and (b) wide-angle scattering measurements. The *d*-spacings labelled with an Asterix refer to peaks corresponding to the Cub_{bi} phase ($Ia\bar{3}d$ symmetry).

formation of a cubic phase for compound **6** was unexpected, as previously prepared Cub_{bi} phases of CD derivatives were observed at lower volume fractions (between f = 0.35 and 0.39).[18] This difference may arise from the use of branched chains in the present systems, which is expected to impact not only the relative volumes of the hydrophilic and hydrophobic domains, but also the overall molecular shape, and therefore the mode of self-assembly. The range of volume fractions over which the cubic phase is stable will also be sensitive to the segment–segment interaction energy, χ,[21,22] which is expected to vary with branching. Indeed, in their comparison of Janus dendrimers with similar volume fractions but differing levels of branching, Choi and coworkers found that only the more highly branched system formed a cubic phase.[34] The unexpected observation of a Cub_{bi} phase for compound **6** underscores a limitation of the group additivity approach, which appears to be less reliable for calculating volume fractions in cases where branched chains are present. More rigorous (and computationally intensive) approaches such as molecular dynamics simulations may be warranted in the future to better understand these systems.

Table 2 Phase behaviour of compounds **3–7**

Compound	Heating phase[a] T (°C)[a] [ΔH (J g^{-1})][b] phase[a]	Cooling phase[a] T (°C)[a] [ΔH (J g^{-1})][b] phase[a]
3 (C_6)	Iso[c]	Iso[c]
4 (C_8)	Iso[c]	Iso[c]
5 (C_{10})	SmA 47.6 [0.662] Iso	Iso 37.9 [−0.581] SmA
6 (C_{12})	SmA/Cub_{bi} 64.9 [0.684] Iso	Iso 58.9 [−0.645] SmA/Cub_{bi}
7 (C_{18})	Cr–Sm 58.6 [38.8] SmA 89.61 [0.634] Iso	Iso 85.9 [−0.631] SmA 50.4 [−36.7] Cr–Sm

[a] Phases identified by POM and XRD experiments: Cr–Sm = solid smectic, SmA = smectic A, Cub_{bi} = bicontinuous cubic ($Ia\bar{3}d$ symmetry), Iso = isotropic. [b] Cransition temperatures and enthalpies were determined by DSC (scan rate = 10 °C min^{-1}) on the second heating/cooling cycle. [c] Isotropic at room temperature by POM and XRD experiments; no phase transitions were observed between 0 and 100 °C using DSC.

A notable trend across this series is the significant decrease of the clearing temperature, T_c, with shortening of the aliphatic chains, from 90 °C for **7** (C_{18}) to 65 °C for **6** (C_{12}) and 48 °C for **5** (C_{10}). The loss of liquid crystallinity for **4** (C_8) and **3** (C_6) can be understood as being due to the further destabilization of the liquid crystal phase at still shorter chains lengths. This trend likely reflects the decreasing shape anisotropy of the mesogens as the aliphatic chains are shortened. Overall the molecular length decreases from 48 Å for **7** to 33.6 Å for **3**, the mesogens become progressively less rod-like (Fig. 4), which is a key predictor of clearing temperature in small molecule liquid crystals.

DSC, POM and solid-state NMR studies of composite 7 (C_{18})–Li

Compound **7** was selected to prepare a lithium-doped composite because it contains the same C18 chains as previously

reported compound **2**; thus, it can be used as benchmark for comparison. The lithium-doped composite **7** (C_{18})–Li was prepared by mixing compound **7** (C_{18}) with LiTFSI at a 1 : 11 ratio which represents 35.7% (w/w) of LiTFSI in the composite. The selection of 11 equivalents of LiTFSI was based on its alignment with the established [1 : 5] ratio of lithium to ethylene glycol (EO) units as done in the related work.[16] DSC of the 7 (C18)–Li composite exhibits a single large enthalpy (30.6 J g^{-1}) transition at 62.2 °C on heating (Fig. S40), with no further transitions observed between 0 °C and 250 °C. A corresponding transition is observed at 50.3 °C upon cooling. The enthalpy and hysteresis for this peak is strongly suggestive of a melting transition. Observations by polarized optical microscopy confirm this assignment: at 62 °C, the solid sample melts to a birefringent liquid. This liquid crystal phase clears to an isotropic liquid over a 2–3 degree range at approximately 235 °C. The failure to observe this clearing transition by DSC is likely due to a combination of its breadth and low enthalpy. Upon cooling, this sample initially forms bâtonnets, which merge into the fan texture of a SmA phase (Fig. S45). This texture remains stable until the freezing transition, when we observe a loss of fluidity and a dramatic increase in birefringence (Fig. S45). Notably, while neat compound **7** (C_{18}) melts at a similar temperature (58.6 °C) to the lithiated sample, it clears at a much lower temperature (89.6 °C); doping LiTFSI leads to a dramatic stabilization of the mesophase.

Solid-state ^{1}H and ^{13}C magic-angle spinning (MAS) NMR spectroscopy were performed on compound **7** (C_{18}) and its lithium composite **7** (C_{18})–Li, to examine any structural changes brought on by addition of lithium. Sharper resonances arise between 0 and 10 ppm in the ^{1}H MAS NMR spectrum of the lithium composite showing improved ^{1}H resolution following by Li addition, and were buried in **7** (C_{18}) due to the stronger ^{1}H–^{1}H dipolar coupling. The sharper and more resolved resonances support an increase in local dynamics, whereby local motions can assist in attentuating the strong ^{1}H homonuclear dipolar coupling (Fig. 7a). The ^{13}C{^{1}H} cross-polarization (CP) MAS NMR spectra of parent **7** (C_{18}) and Li^{+} incorporated **7** (C_{18})–Li show nearly identical signals in the aliphatic region (0 and 80 ppm), with the exception of **7** (C_{18}). The ^{13}C peak at 71.5 ppm (OCH_2 groups of the *O*-monomethyl triethylene glycol groups) shows a lower frequency shift to 69.9 ppm with decreased intensity and slight broadening upon Li^{+} addition (Fig. 7b), supporting an interaction of Li^{+} ions with the *O*-monomethyl triethylene glycol groups, and that the overall backbone structure remains unaltered with Li^{+} incorporation.

The variable-temperature (VT, 296 K to 344 K) ^{7}Li MAS NMR was measured on **7** (C_{18})–Li, and the entire examined temperature range showed a sharp single ^{7}Li NMR resonance (Fig. 7c). Careful analysis of the resonance reveals that a slight change in isotropic chemical shift (from −1.10 to −0.93 ppm) towards the higher frequency region (Fig. 7d) occurs with increasing

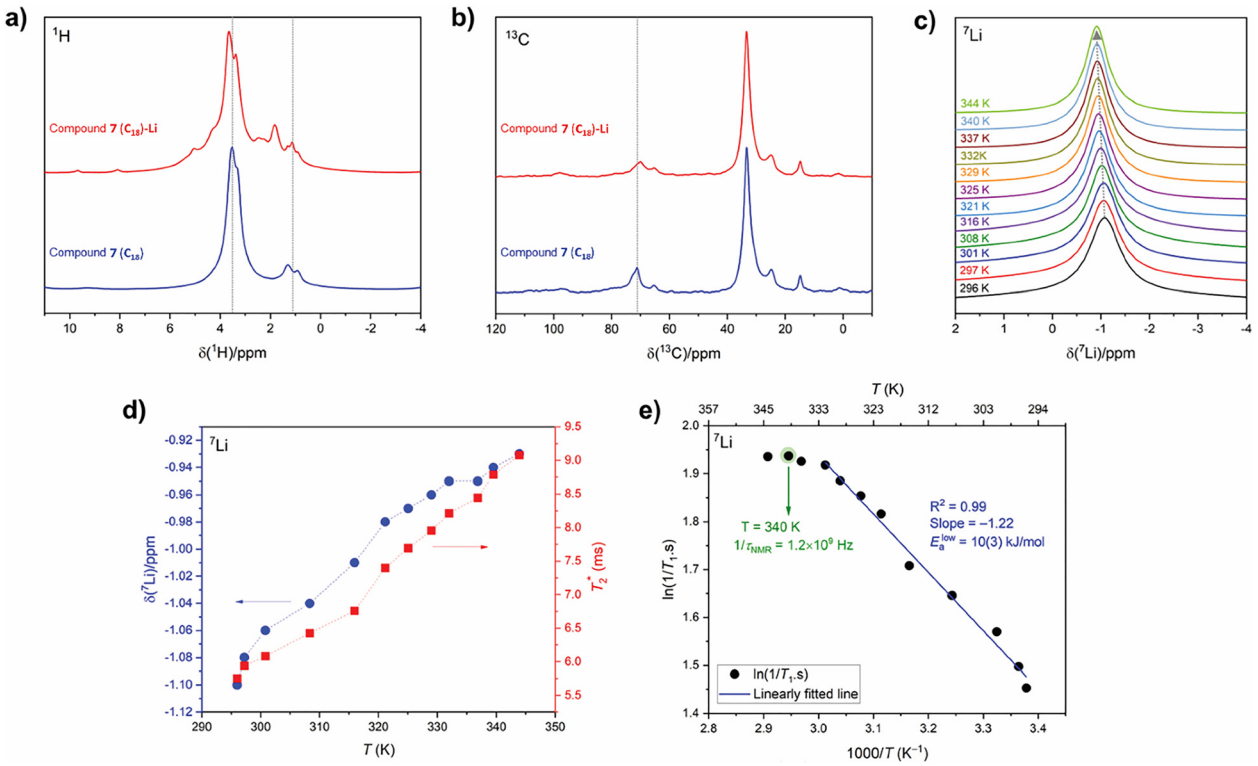

Fig. 7 Room temperature (a) ^{1}H and (b) ^{13}C{^{1}H} CP MAS NMR spectra of compounds **7** (C_{18}) and **7** (C_{18})–Li; the dashed lines act as guides to the eye. (c) ^{7}Li MAS NMR spectra of **7** (C_{18})–Li recorded at variable temperatures (296 to 344 K) with the dotted line showing higher frequency shift of peak maxima; and the dependence of corresponding (d) ^{7}Li isotropic chemical shifts (δ) and T_2^* as a function of temperature. (e) Temperature dependence of ^{7}Li nuclear spin–lattice relaxation rates ($1/T_1$); the rate maximum was found at $T \approx 340$ K with an activation energy of the low-temperature side as 10(3) kJ mol^{-1}.

temperature. This is complemented by a narrowing of the ^{7}Li NMR resonances (from 174 to 110 Hz). These spectral changes support an increase in local Li^{+} mobility, whereby a reduction in the linewidth is associated with a reduction in the residual dipolar coupling of neighbouring ^{1}H and ^{7}Li nuclear spins (*i.e.*, increase in the spin–spin lattice relaxation (T_2^*), Fig. 7d).

The thermally activated regions of Li-ion dynamics in compound 7 (C_{18})–Li were assessed by performing variable-temperature ^{7}Li nuclear spin–lattice (T_1) relaxometry using an Arrhenius representation and the spin–lattice relaxation (SLR) rates ($1/T_1$) were measured and are plotted in Fig. 7e. A diffusion-induced relaxation rate peak having a characteristic low-temperature flank was observed with its maximum located at a $T \approx 340$ K, and a mean jump rate ($1/\tau_{NMR}$) of Li-ions = 1.2×10^{9} Hz at this temperature was obtained from the relation $\omega_0.\tau_{NMR} \approx 1$ at the SLR maximum,[35] where the value of angular Larmor frequency (ω_0) was used from the equation $\omega_0/2\pi(^{7}\text{Li})$ = 194.42 MHz. The calculated $1/\tau_{NMR}$ falls in the GHz regime, and such fast Li-ion exchange processes suggest high ionic conductivity or fast local Li-ion hopping. The low-temperature flank ($\omega_0.\tau_{NMR} \gg 1$) of the diffusion-induced rate peak is sensitive towards the local Li-ion hopping processes, and an activation energy (E_a^{low}) of 10(3) kJ mol^{-1} was obtained from the slope of this regime, which is typically influenced by the correlation effects, such as structural disorder or coulombic interactions.[35]

Impedance studies of composite 7 (C_{18})–Li

Ionic conductivities of composite 7 (C_{18})–Li were assessed through electrochemical impedance spectroscopy (EIS) using a custom 2-probe cell equipped with titanium electrodes. Impedance spectra were acquired at the open-circuit potential using a 100 mV AC perturbation over 0.1 Hz–0.1 MHz, with measurements conducted at 50–200 °C.

Nyquist plots ($-Z''$ as a function of Z') were generated using CHI650C Electrochemical Workstation software, and sample plots at 90 °C, 110 °C and 130 °C are shown in Fig. 8a. All of the plots exhibited a high-frequency semi-circle followed by a low-frequency linear tail with a slope nearing 45°, attributable to diffusion processes.[36] The obtained data were fitted using an $(RQ)(Q)$ equivalent circuit, where R represents resistance, and Q is a constant-phase element. All impedance data were fit to the same equivalent circuit, and the R-value was used in the conductivity assessments, according to the equation given below:

$$\sigma = \frac{l}{a} \times \frac{1}{R}$$

where l is the thickness of the sample (cm) and a is the area of the electrode (cm^2).

The SI (Fig. S55 and S56) includes Nyquist plots obtained at various temperatures. Consistent with expectations, the resistance shows an inverse relationship with temperature, and the calculated Li^{+} conductivity increases steadily with increasing temperature, reaching a maximum of 4.86×10^{-3} S cm^{-1} at 200 °C (Table S1). The activation energy (E_a) of the ion-conductive process, as determined from the Arrhenius-type plot ($\log(\sigma T)$ plotted against $1000/T$) during both heating and cooling cycles, averaged 0.31 eV (Fig. 8b). The electrochemical impedance spectroscopy yielded a much higher activation energy compared to the activation energy derived from solid-state ^{7}Li-NMR of 7 (E_a = 0.09 eV). The difference in activation energies obtained from solid-state NMR and EIS is expected and arises from the distinct length and time scales probed *via* these techniques. EIS measures long-range ionic transport through the bulk material under an applied electric field and therefore reflects the higher energy barriers associated with continuous diffusion pathways governed by the material's structural connectivity. In contrast, NMR probes local ^{7}Li dynamics on atomic length scales, yielding lower activation energies that capture short-range vibrations, site-to-site hopping or back-and-forth motions that do not necessarily contribute to net ionic conduction. Consequently, NMR-derived activation energies reflect local Li-ion mobility within the structural framework, whereas EIS-derived values reflect the effective barriers governing macroscopic ion transport.

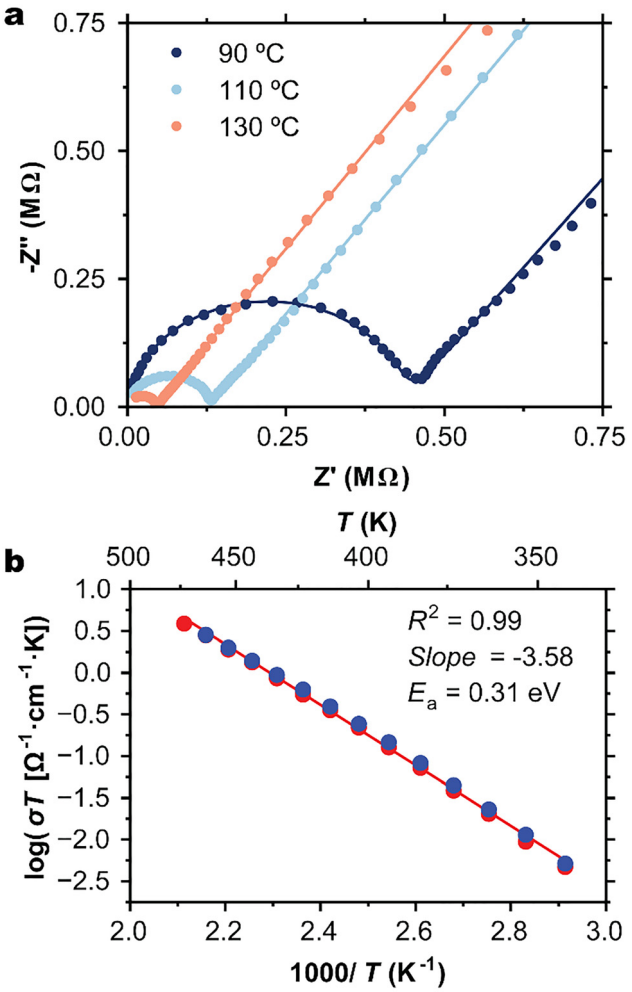

Fig. 8 (a) Nyquist plot of compound **7** (C_{18})–Li at 90 °C (blue), 110 °C (light blue), and 130 °C (orange) on the second heating cycle including the equivalent circuit used in the fitting (blue, light blue, and orange line) of the raw data (circles). (b) Arrhenius-type plot of the conductivity (normalised for sample area and thickness) of the lithiated sample as a function of temperature overlayed with the best fit linear equation (red line).

The results of impedance experiments compare favourably to a previously reported compound that contains 14 *O*-cyanoethyl-functionalized triethylene glycol chains at the secondary face (*i.e.* persubstituted at all O_2 and O_3-positions) and 7 octadecyl chains at the primary face of β-CD;[17] despite its higher hydrophilic fraction volume, impedance studies showed that it had a higher activation energy (E_a =0.57 eV). This suggests an enhancement of conductivity for the current system. The improvement could be primarily attributed to the increased number of EO chains introduced into the primary face of our β-CD for easier Li^+ mobility.

C Conclusions

We report the innovative design and synthesis of a new class of liquid crystalline electrolytes based on biodegradable amphiphilic cyclodextrin derivatives. Compared to previously reported analogs, we successfully doubled the number of ion-conducting oligoethylene glycol chains on the primary face by leveraging epichlorohydrin chemistry, yielding amphiphilic CDs with approximately cylindrical geometries. This is a new class of cyclodextrin mesogens, which are monodisperse, readily isolated, and well-characterized. As predicted, the increase in hydrophilic volume fraction drove self-assembly from columnar (unbranched) to lamellar (branched). Unexpectedly, one derivative exhibited the coexistence of SmA and Cub_{bi} phases, and the two shortest analogs were isotropic at all temperatures examined. Impedance spectroscopy measurements on lithium doped compound **7** (C_{18}) show a lower activation energy that compares favorably to a previous analog containing the same number of oligoethylene glycol chains but half the number of aliphatic chains. The modularity of our synthetic approach enables facile functionalization, and thus should offer a versatile platform for the development of next-generation CD-based LC electrolytes with improved ionic conductivity and thermal stability. This work underscores the promise of amphiphilic CD-based architectures for advancing ion transport technologies and should inspire further exploration in this emerging field.

D Experimental section

Methods

Chemical synthesis. β-Cyclodextrin was purchased from Wacker Chemie. Unless otherwise stated, all commercial reagents were used without further purification. Analytical thin layer chromatography was performed on Silica Gel 60-F_{254} TLC Plates (Sigma-Aldrich®), *via* detection by quenching of fluorescence and/or by charring with either 5% aqueous sulfuric acid or a ceric ammonium molybdate dip. Column chromatography purification was performed on Silica Gel 60 (Silicycle, Ontario). Organic solutions were concentrated under reduced pressure with the assistance of a water bath at <60 °C. 1D and 2D ^{1}H and ^{13}C NMR spectra were recorded on a Bruker Advance III 400 MHz spectrometer equipped with a BBFO probe. Chemical shifts were reported in δ (ppm) and referenced to residual $CHCl_3$ (δ_H 7.24) and $CDCl_3$ (δ_C 77.0, $CDCl_3$). First order coupling constants were reported in Hz for ^{1}H nuclei. The ^{1}H and ^{13}C NMR spectra were assigned with the assistance of DEPTQ, gCOSY, and gHSQC experiments. High resolution ESI-QTOF mass spectra were recorded on an Agilent 6520 Accurate Mass Quadrupole Time-of-Flight LC/MS spectrometer.

DSC. Differential scanning calorimetry experiments were performed on a PerkinElmer DSC 6000. Unless otherwise stated, all runs were carried out at a heating/cooling rate of 10 °C min^{-1}, with a one-minute isothermal equilibration at the end of each cycle.

POM. Polarized optical microscopy experiments were carried out using an Olympus BX50 microscope equipped with a Nikon D90 DSLR camera. Sample temperatures were controlled using a Linkam LTS350 heating stage coupled with a TMS94 temperature controller.

XRD. The experiments were conducted on a SAXSLAB Ganesha 300XL small angle X-ray scattering (SAXS) instrument (Cu source, 45 kV, 0.6 mA). All samples were loaded into thin-walled quartz capillary tubes (Charles Supper Company) with an outer diameter of 1.5 mm. All measurements were performed on a Linkam T95-PE heating stage. Each spectrum was collected for 8 minutes.

Solid-state NMR spectroscopy. A Bruker AVANCE NEO 500 NMR spectrometer was used to conduct solid-state ^{1}H, ^{13}C, and ^{7}Li NMR experiments equipped with a high field superconducting magnet (B_0 = 11.75 T) and a 4 mm double-resonance (H/X) Bruker magic-angle spinning (MAS) probe. For measurements at room and variable temperatures (VT), powdered samples were packed into 4 mm (outside diameter) zirconia rotors and sealed using Kel-F or Vespel caps, respectively. Topspin 4.1.1 Bruker software was used to process all NMR data, and Origin 2021 software was used to plot the results.

(i) ^{1}H MAS NMR. A Bloch pulse sequence[37] with a 4 μs π/2 pulse ($\omega_1/2\pi$ = 62.5 kHz), an optimized recycle delay of 3 s, 4 co-added transients, and a 4 kHz MAS frequency were used to record the ^{1}H NMR spectra ($\omega_0/2\pi(^1H)$ = 500.27 MHz). The ^{1}H NMR data were referenced to adamantane at $\delta(^1H)$ = 1.85 ppm with respect to TMS $\delta(^1H)$ at 0 ppm.

(ii) ^{13}C Cross-polarization MAS (CPMAS)[38] NMR. The $^{13}C\{^1H\}$ CPMAS NMR spectra ($\omega_0/2\pi(^{13}C)$ = 125.80 MHz) were recorded by optimizing the Hartman–Hahn[39] matching condition on ^{13}C and optimizing the contact time (2.0 or 1.5 ms for compound **7** (C_{18}) and its lithium composite **7** (C_{18})–Li samples, respectively), recycle delay of 3 s, 256 co-added transients, and a 4 kHz MAS frequency by applying a 4 μs Bloch decay (π/2) pulse ($\omega_1/2\pi$ = 62.5 kHz) on ^{1}H. The ^{13}C NMR data were referenced to adamantane ^{13}C higher frequency peak at $\delta(^{13}C)$ = 38.56 ppm with respect to TMS $\delta(^{13}C)$ at 0 ppm.

(iii) ^{7}Li Variable temperature (VT) MAS NMR. VT (296 to 344 K) ^{7}Li MAS NMR spectra ($\omega_0/2\pi(^7Li)$ = 194.42 MHz) were acquired using a 4 μs Bloch decay (π/2) pulse ($\omega_1/2\pi$ = 62.5 kHz), an optimized recycle delay of 2 s, 16 co-added transients, and spinning frequencies of 4 to 7 kHz by controlling the

temperatures using a Bruker VT unit, and the sample temperatures were corrected for frictional heating and instrument calibration using $CH_3NH_3PbCl_3$ powder.[40] All ^{7}Li NMR data were referenced to LiCl (1M) at $\delta(^7\text{Li}) = 0$ ppm.

The ^{7}Li nuclear spin–lattice relaxation time (T_1) was measured using an inversion recovery pulse sequence ($\pi - \tau_D - \pi/2$ − ACQ, where τ_D is the variable delay). The ^{7}Li peak areas were fitted using a single-exponential decay function: $A_t = A_\infty + Ce^{-t/T_1}$ (where A_t and A_∞ are the NMR peak areas recorded at time t and infinity, respectively, and C is the pre-exponential constant) to yield the ^{7}Li T_1 values.

Compounds **21–22** were prepared as previously published.[17]

2,5,8,11,15,18,21,24-Octaoxapentacosan-13-ol (10)

To neat *O*-monomethyl triethylene glycol (**9**, 4.50 g, 0.027 mol, 2.0 equiv.) under an argon atmosphere, was added sodium hydride (1.10 g, 0.046 mol, 2.1 equiv.) and solution was stirred for 10 min. Epichlorohydrin (1.1 g, 0.012 mol, 1.0 equiv.) was then added and the solution was heated to 100 °C overnight. MeOH was added to quench the reaction and the solution was concentrated under reduced pressure. The crude mixture was purified by column chromatography on silica gel using a gradient of MeOH–EtOAc (1 → 10%) as the eluent. The desired compound **10** was isolated as a syrup (1.33 g, 3.46 mmol, 32% yield). R_f = 0.19 (MeOH : EtOAc, 5 : 95). ^{1}H NMR (400 MHz, $CDCl_3$) δ 3.92 (m, 1H, $OCH_2CH(O)CH_2O$), 3.56–3.67 (m, 20H, 10 × OCH_2), 3.42–3.55 (m, 8H, 2 × OCH_2 + $OCH_2CH(O)CH_2O$), 3.33 (s, 6H, 2 × OCH_3). ^{13}C NMR (400 MHz, $CDCl_3$) δ 72.5 (OCH_2), 71.9 (OCH_2), 70.8 (OCH_2), 70.5 (OCH_2), 70.5 (OCH_2), 69.4 ($OCH_2CH(O)CH_2O$), 59.0 (2 × OCH_3).

13-(Prop-2-ynyloxy)-2,5,8,11,15,18,21,24-octaoxapentacosane (11)

To a solution of compound **10** (1.33 g, 4.6 mmol) in THF (10 mL) under an atmosphere of argon, was added sodium hydride (0.28 g, 0.012 mol, 2.0 equiv.), and the mixture was stirred for 10 min. Propargyl bromide (1.03 g, 8.66 mmol, 2.0 equiv.) was added, and the reaction mixture was stirred overnight. The reaction was quenched with MeOH and the mixture was concentrated under reduced pressure. The crude mixture was then purified by column chromatography on silica gel using EtOAc as the eluent to afford the desired compound **11** as a syrup (1.0 g, 2.36 mmol, 68% yield). R_f = 0.21 (100% EtOAc). ^{1}H NMR (400 MHz, $CDCl_3$) δ 4.32 (d, J = 2.4 Hz, 2H, $OCH_2C{\equiv}CH$), 3.85 (ddd, 1H, J = 4.7, 5.6, 10.3 Hz, $OCH_2CH(O)CH_2O$), 3.59–3.67 (m, 20H, 10 × OCH_2), 3.50–3.59 (m, 8H, 2 × OCH_2 + $OCH_2CH(O)CH_2O$), 3.35 (s, 6H, 2 × OMe), 2.40 (t, J = 2.4 Hz, 1H, $OCH_2C{\equiv}CH$). HRMS (ESI) m/z $[C_{20}H_{38}O_9 + NH_4]^+$ calc.: 440.2854, found: 440.2858.

Heptakis[6-azido-6-deoxy-2,3-di-*O*-hexanoyl]cyclomaltoheptaose (18)

To a solution of β-CD heptaazide **12** (5.0 g, 3.8 mmol, 1.0 equiv.) in anhydrous toluene (200 mL), hexanoic anhydride (**13**, 22.9 g, 0.107 mol, 2.0 equiv./OH), prepared by reacting hexanoic acid (24.8 g, 0.21 mol) with DCC (11.0 g, mol) as previously reported,[17] was added along with 4-dimethylaminopyridine (DMAP) (13.0 g, 0.11 mol, 2.0 equiv./OH), and the reaction mixture was stirred under argon at 70 °C overnight. The crude reaction mixture was then concentrated under reduced pressure. The crude mixture was then dissolved in a mixture of CH_2Cl_2/MeOH (10 : 90), and the desired compound **18** precipitated out from the solution. After filtration, compound **18** (7.66 g, 2.80 mmol) was isolated in 75% yield. R_f = 0.30 (CH_2Cl_2). ^{1}H NMR (400 MHz, $CDCl_3$) δ 5.33 (dd, J = 8.5, 9.8 Hz, 7H, 7 × H-3), 5.09 (d, J = 3.8 Hz, 7H, 7 × H-1), 4.85 (dd, J = 3.8, 9.8 Hz, 7H, 7 × H-2), 4.02 (ddd, J = 9.5, 4.4, 1.8 Hz, 7H, 7 × H-5), 3.80–3.71 (m, 14H, 7 × H-6a + 7 × H-4), 3.65 (dd, J = 13.7, 4.9 Hz, 7H, 7 × H-6b), 2.46–2.12 (m, 28H, 14 × CH_2CO), 1.71–1.49 (m, 28H, 14 × CH_2CH_2CO), 1.43–1.21 (m, 56H, 14 × $(CH_2)_2CH_3$), 0.94 (t, J = 6.7 Hz, 21H, 7 × CH_3), 0.92 (t, J = 6.7 Hz, 21H, 7 × CH_3). ^{13}C NMR (101 MHz, $CDCl_3$) δ 173.22, 171.72, 96.36, 76.66, 70.77, 70.07, 51.55, 39.38, 33.98, 33.76, 31.38, 31.25, 24.35, 24.31, 22.35, 13.87. HRMS (ESI) m/z $[C_{126}H_{203}N_{21}O_{42} + NH_4]^+$ calc.: 2700.4733, found: 2700.4636.

Heptakis[6-azido-6-deoxy-2,3-di-*O*-octanoyl]cyclomaltoheptaose (19)

To a solution of β-CD heptaazide **12** (1.37 g, 1.1 mmol, 1.0 equiv.) in anhydrous toluene (100 mL), octanoic anhydride (**14**, 7.92 g, 29.3 mmol, 2.0 equiv./OH), prepared by reacting octanoic acid (8.45 g, 0.59 mol) with DCC (6.04 g, 0.14 mol) as previously reported,[17] was added along with 4-dimethylaminopyridine (DMAP) (3.58 g, 29.3 mmol, 2.0 equiv./OH), and the reaction mixture was stirred under argon at 70 °C overnight. The crude reaction mixture was then concentrated under reduced pressure. The crude mixture was then dissolved in a mixture of CH_2Cl_2/MeOH (10 : 90), and the desired compound **19** precipitated out in the solution. After filtration, compound **19** (3.18 g, 1.03 mmol) was isolated in 97% yield. R_f = 0.34 (CH_2Cl_2). 1H NMR (400 MHz, CDCl3) δ 5.30 (dd, J = 10.1, 8.5 Hz, 7H, 7 × H-3), 5.05 (d, J = 3.9 Hz, 7H, 7 × H-1), 4.79 (dd, J = 10.1, 3.8 Hz, 7H, 7 × H-2), 3.99 (ddd, J = 9.8, 4.7, 2.3 Hz, 7H, 7 × H-5), 3.75–3.69 (m, 14H, 7 × H-6a + 7 × H-4), 3.65 (dd, 7H, 7 × H-6b), 2.43–2.12 (m, 28H, 14 × CH_2CO), 1.67–1.47 (m, 28H, 14 × CH_2CH_2CO), 1.36–1.19 (m, 112H, 28 × $(CH_2)_2CH_3$), 0.91 (t, J = 6.7 Hz, 42H, 14 × CH_3). ^{13}C NMR (101 MHz, CDCl3) δ 173.2, 171.7, 96.4, 76.7, 70.77, 70.07, 51.6, 39.4, 33.98, 33.76, 31.4, 31.3, 24.35, 24.31, 22.35, 13.87. HRMS (ESI) m/z $[C_{154}H_{259}N_{21}O_{42} + NH_4]^+$ calc.: 3092.9115, found: 3092.8946.

Heptakis[6-azido-6-deoxy-2,3-di-*O*-decanoyl]cyclomaltoheptaose (20)

To a solution of β-CD heptaazide **12** (0.48 g, 0.37 mmol, 1.0 equiv.) in anhydrous toluene (50 mL), decanoic anhydride (**15**, 3.35 g, 10.2 mmol, 2.0 equiv./OH), prepared by reacting decanoic acid (3.53 g, 20.5 mmol) with DCC (2.12 g, 10.2 mmol) as previously reported,[17] was added along with 4-dimethylaminopyridine (DMAP) (1.25 g, 10.2 mmol, 2.0 equiv./OH), and the reaction mixture was stirred under argon at 70 °C overnight. The crude reaction mixture was then concentrated under reduced pressure. The crude mixture was then dissolved in a mixture of CH_2Cl_2/MeOH (10 : 90), and the desired compound **20** precipitated out in the solution. After filtration,

compound **20** (1.23 g, 0.36 mmol) was isolated in 98% yield. R_f = 0.36 (CH_2Cl_2). ^{1}H NMR (400 MHz, $CDCl_3$) δ 5.30 (dd, J = 10.0, 8.5 Hz, 7H, 7 × H-3), 5.06 (d, J = 3.8 Hz, 7H, 7 × H-), 4.79 (dd, J = 10.1, 3.8 Hz, 7H, 7 × H-2), 4.00 (ddd, J = 9.7, 4.7, 2.3 Hz, 7H, 7 × H-5), 3.78–3.68 (m, 14H, 7 × H-6a + 7 × H-4), 3.67–3.57 (m, 7H, 7 × H-6b), 2.42–2.11 (m, 28H, 14 × CH_2CO), 1.66–1.47 (m, 28H, 14 × CH_2CH$_2$CO), 1.34–1.21 (m, 168H, 28 × (CH_2)$_2$CH$_3$), 0.88 (t, J = 6.9 Hz, 42H, 14 × CH_3). ^{13}C NMR (101 MHz, $CDCl_3$) δ 173.2, 171.7, 96.3, 76.6, 70.74, 70.16, 70.08, 51.6, 34.1, 33.8, 31.9, 29.7, 29.58, 29.55, 29.43, 29.39, 29.27, 24.79, 24.71, 22.7, 14.1. HRMS (ESI) m/z [$C_{182}H_{315}N_{21}O_{42}$ + 2NH_4]$^{2+}$ calc.: 1751.6918, found: 1751.6817.

Heptakis{6-deoxy-6-[4-(3-2,5,8,11-tetraoxadodecyl-2,5,8,11,14-pentaoxapentadecyl)-1*H*-1,2,3-triazol-1-yl]-2,3-di-*O*-hexanoyl}cyclomaltoheptaose (3)

To a solution of compound **18** (0.250 g, 0.09 mmol, 1.0 equiv.) in acetone (10 mL), compound **11** (0.54 g, 1.28 mmol, 2.0 equiv./OH), DIPEA (0.011 mL, 0.062 mmol, 0.05 equiv.) and CuI (1.2 mg) were added. The reaction was heated to 50 °C under argon for 4 days. The reaction mixture was concentrated under reduced pressure. The solid residue was dissolved in EtOAc (50 mL) and the organic solution was washed with saturated aqueous EDTA solution (2 × 30 mL), dried over anhydrous Na_2SO_4, and evaporated. The crude mixture was purified *via* precipitation in a mixture (200 mL) of toluene/hexane (10 : 90, 20/180 mL) to afford the desired product **3** which was isolated as a waxy solid (0.240 g, 0.040 mmol, 51% yield). R_f = 0.82 (MeOH: CH_2Cl_2, 15 : 85). ^{1}H NMR (400 MHz, $CDCl_3$) δ 7.79 (br s, 7H, 7 × 1,2,3-triazole), 5.51 (br s, 7H, 7 × H-1), 5.40 (br dd, J = 9.0, 9.0 Hz, 7H, 7 × H-3), 4.74–4.94 (br, 14H, 7 × H-6a + 7 × H-6b), 4.57–4.77 (br, 21H, 7 × 1,2,3-triazole-CH_2O + 7 × H-2), 4.47 (br, 7H, 7 × H-5), 3.88–3.43 (m, 210H, 7 × OCH$_2$CH(O)CH$_2$O + 84 × OCH$_2$ + 7 × H-4), 3.38 (br s, 42H, 14 × OMe), 2.51–2.06 (m, 28H, 14 × CH_2CO), 1.67–1.46 (m, 28H, 14 × CH_2CH$_2$CO), 1.15–1.45 (m, 56H, 14 × CH$_3$(CH_2)$_2$), 0.90 (t, J = 6.9 Hz, 42H, 14 × CH_3). ^{13}C NMR (101 MHz, $CDCl_3$) δ 173.04, 171.68, 125.63, 77.75, 71.91, 71.15, 70.76, 70.57, 70.52, 70.48, 69.66, 63.73, 59.00, 33.94, 33.73, 31.43, 31.23, 24.31, 24.26, 22.41, 13.90. HRMS (ESI) m/z [$C_{266}H_{469}N_{21}O_{105}$ + 3Na]$^{3+}$ calc.: 1902.3894, found: 1902.3847.

Heptakis{6-deoxy-6-[4-(3-2,5,8,11-tetraoxadodecyl-2,5,8,11,14-pentaoxapentadecyl)-1*H*-1,2,3-triazol-1-yl]-2,3-di-*O*-octanoyl}cyclomaltoheptaose (4)

To a solution of compound **19** (0.170 g, 0.055 mmol, 1.0 equiv.) in acetone (15 mL), was added compound **11** (0.33 g, 0.77 mmol, 2.0 equiv./OH), DIPEA (0.010 mL, 0.057 mmol, 0.7 equiv.) and CuI (3.2 mg), and the reaction was heated to 50 °C under argon for 2 days. The reaction mixture was concentrated under reduced pressure, and the solid residue was dissolved in EtOAc (50 mL); the organic solution was washed with saturated aqueous EDTA solution (2 × 30 mL), dried over anhydrous Na_2SO_4, and evaporated. The crude mixture was purified by a precipitation in a mixture (100 mL) of MeOH/H_2O (20 : 80) to afford compound **4** as a waxy solid (0.300 g, 0.05 mmol, 90% yield). R_f = 0.73 (MeOH: CH_2Cl_2, 10 : 90).^{1}H NMR (400 MHz, $CDCl_3$) δ 7.77 (br s, 7H, 7 × 1,2,3-triazole), 5.51 (br s, 7H, 7 × H-1), 5.39 (br dd, 7H, 7 × H-3), 4.87–4.81 (br s, 14H, 7 × H-6a + 7 × H-6b), 4.75–4.62 (br, 21H, 7 × 1,2,3-triazole-CH_2O + 7 × H-2), 4.47 (br, 7H, 7 × H-5), 3.88–3.43 (m, 210H, 7 × OCH_2CH(O)-CH_2O + 84 × OCH$_2$ + 7 × H-4), 3.36 (br s, 42H, 14 × OMe), 2.51–2.06 (m, 28H, 14 × CH_2CO), 1.61–1.46 (m, 28H, 14 × CH_2CH$_2$CO), 1.34–1.20 (m, 112H, 14 × (CH_2)$_2$CH$_3$), 0.88 (t, J = 6.9 Hz, 42H, 14 × CH_3). ^{13}C NMR (101 MHz, $CDCl_3$) δ 173.0, 171.7, 145.3, 125.6, 96.3, 77.8, 71.92, 71.16, 71.11, 70.77, 70.75, 70.58, 70.53, 70.48, 70.45, 69.7, 63.8, 59.0, 34.1, 33.8, 31.9, 31.8, 29.69, 29.38, 29.20, 29.18, 24.72, 24.64, 22.7, 14.0. HRMS (ESI) m/z [$C_{294}H_{525}N_{21}O_{105}$ + 3Na]$^{3+}$ calc.: 2033.2021, found: 2294.1988.

Heptakis{6-deoxy-6-[4-(3-2,5,8,11-tetraoxadodecyl-2,5,8,11,14-pentaoxapentadecyl)-1*H*-1,2,3-triazol-1-yl]-2,3-di-*O*-decanoyl}cyclomaltoheptaose (5)

To a solution of compound **20** (0.250 g, 0.072 mmol, 1.0 equiv.) in acetone (15 mL), was added compound **11** (0.43 g, 1.0 mmol, 2.0 equiv./N_3), DIPEA (0.010 mL, 0.058 mmol, 0.8 equiv.) and CuI (2.8 mg), and the reaction was heated to 50 °C under argon for 2 days. The reaction mixture was concentrated under reduced pressure, and the solid residue was dissolved in EtOAc (50 mL); the organic solution was washed with saturated aqueous EDTA solution (2 × 30 mL), dried over anhydrous Na_2SO_4, and evaporated. The crude mixture was purified by a precipitation in a mixture (100 mL) of MeOH/H_2O (20 : 80) to afford compound **5** as a waxy solid (0.385 g, 0.06 mmol, 82% yield). R_f = 0.72 (MeOH: CH_2Cl_2, 10 : 90).^{1}H NMR (400 MHz, $CDCl_3$) δ 7.78 (br s, 7H, 7 × 1,2,3-triazole), 5.49 (br s, 7H, 7 × H-1), 5.39 (br dd, 7H, 7 × H-3), 4.87–4.81 (br s, 14H, 7 × H-6a + 7 × H-6b), 4.76–4.58 (br, 21H, 7 × 1,2,3-triazole-CH_2O + 7 × H-2), 4.47 (br, 7H, 7 × H-5), 3.88–3.43 (m, 210H, 7 × OCH_2CH(O)-CH_2O + 84 × OCH$_2$ + 7 × H-4), 3.36 (br s, 42H, 14 × OMe), 2.42–2.08 (m, 28H, 14 × CH_2CO), 1.67–1.44 (m, 28H, 14 × CH_2CH$_2$CO), 1.34–1.20 (m, 168H, 14 × (CH_2)$_2$CH$_3$), 0.88 (t, J = 6.3 Hz, 42H, 14 × CH_3). ^{13}C NMR (101 MHz, $CDCl_3$) δ 77.7, 76.1, 71.91, 71.14, 70.76, 70.58, 70.48, 59.0, 32.69, 31.97, 29.65, 29.51, 27.4, 24.7, 22.7, 14.1. HRMS (ESI) m/z [$C_{332}H_{581}N_{21}O_{105}$ + 3H]$^{3+}$ calc.: 2142.0329, found: 2142.0192.

Heptakis{6-deoxy-6-[4-(3-2,5,8,11-tetraoxadodecyl-2,5,8,11,14-pentaoxapentadecyl)-1*H*-1,2,3-triazol-1-yl]-2,3-di-*O*-dodecanoyl}cyclomaltoheptaose (6)

To a solution of compound **21** (0.250 g, 0.065 mmol, 1.0 equiv.) in acetone (15 mL), was added compound **11** (0.40 g, 0.95 mmol, 2.0 equiv./OH), DIPEA (0.010 mL, 0.057 mmol, 0.05 equiv.) and CuI (4.3 mg), and the reaction mixture was heated to 50 °C under argon for 2 days. The reaction mixture was concentrated under reduced pressure, and the solid residue was dissolved in EtOAc (50 mL); the organic solution was washed with saturated aqueous EDTA solution (2 × 30 mL), dried over anhydrous Na_2SO_4, and evaporated. The crude mixture was purified by a precipitation in a mixture (200 mL) of MeOH/H_2O (10 : 90) to afford compound **6** as a waxy solid (0.280 g, 0.041 mmol, 68%

yield). R_f = 0.70 (MeOH: CH_2Cl_2, 10 : 90). ^{1}H NMR (400 MHz, $CDCl_3$) δ 7.78 (br s, 7H, 7 × 1,2,3-triazole), 5.50 (br, 7H, 7 × H-1), 5.40 (br dd, J = 8.9, 8.9 Hz, 7H, 7 × H-3), 4.96–4.76 (br, 14H, 7 × H-6a + 7 × H-6b), 4.76–4.53 (br, 21H, 7 × 1,2,3-triazole-CH_2 + 7 × H-2), 4.47 (br, 7H, 7 × H-5), 3.86–3.47 (m, 210H, 7 × $OCH_2CH(O)CH_2O$ + 84 × OCH_2 + 7 × H-4), 3.38 (br s, 42H, 14 × OMe), 2.24–2.06 (m, 28H, 14 × CH_2CO), 1.45–1.67 (m, 28H, 14 × CH_2CH_2CO), 1.39–1.16 (m, 224H, 14 × $CH_3(CH_2)_8$), 0.89 (t, J = 6.9 Hz, 42H, 14 × CH_3). ^{13}C NMR (101 MHz, $CDCl_3$) δ 173.0, 171.7, 145.3, 125.6, 96.4, 77.8, 77.2, 71.9, 71.2, 71.1, 70.8, 70.76, 70.6, 70.5, 70.48, 70.46, 69.7, 63.8, 59.0, 50.0, 34.0, 33.8, 32.0, 29.9, 29.89, 29.83, 29.8, 29.74, 29.7, 29.5, 29.48, 29.3, 24.8, 24.7, 22.7, 14.1. HRMS (ESI) m/z $[C_{350}H_{637}N_{21}O_{105} + 3Na]^{3+}$ calc.: 2294.8276, found: 2294.8220.

Heptakis{6-deoxy-6-[4-(3-2,5,8,11-tetraoxadodecyl-2,5,8,11,14-pentaoxapentadecyl)-1*H*-1,2,3-triazol-1-yl]-2,3-di-*O*-octadecanoyl}cyclomaltoheptaose (7)

To a solution of compound **22** (0.067 g, 0.013 mmol, 1.0 equiv.) in acetone (5.0 mL), was added compound **11** (0.30 g, 0.71 mmol, 2.0 equiv./OH), DIPEA (0.010 mL, 0.057 mmol, 0.05 equiv.) and CuI (0.89 mg), and the reaction mixture was heated to 50 °C under argon for 4 days. The reaction solution was concentrated under reduced pressure, and the solid residue was dissolved in EtOAc (50 mL), and the organic solution was washed with saturated aqueous EDTA solution (2 × 30 mL), dried over anhydrous Na_2SO_4, and evaporated. The crude mixture was purified *via* precipitation in a mixture (200 mL) of CH_2Cl_2/MeOH (10 : 90) to afford the desired product 7 as a light brown solid (0.07 g, 0.0088 mmol, 66% yield). ^{1}H NMR (400 MHz, $CDCl_3$) δ 7.76 (s, 7H, 7 × 1,2,3-triazole), 5.50 (br, 7H, 7 × H-1), 5.40 (br dd, J = 8.5, 8.5 Hz, 7H, 7 × H-3), 4.95–4.49 (br, 14H, 7 × H-6a + 7 × H-6b), 4.69 (br, 21H, 7 × H-2 + 7 × OC*H*a*H*b-1,2,3-triazole), 4.47 (br, 7H, 7 × H-5), 3.88–3.72 (br, 7H, 7 × OCH_2CH(O–)CH_2O), 3.72–3.44 (m, 196H, 84 × OCH_2 + 7 × $OCH_2CH(O)CH_2O$ + 7 × H-4), 3.44–3.32 (br s, 42H, 14 × OMe), 2.50–1.99 (m, 28H, 14 × CH_2CO), 1.54 (br, 28H, 14 × CH_2CH_2CO), 1.38–1.10 (m, 392H, 14 × $CH_3(CH_2)_{14}$), 0.90 (t, J = 6.8 Hz, 42H, 14 × CH_3). ^{13}C NMR (101 MHz, $CDCl_3$) δ 173.0, 171.7, 145.3, 125.6, 96.4, 77.8, 77.2, 71.9, 71.2, 71.1, 70.8, 70.8, 70.6, 70.55, 70.5, 70.48, 69.7, 63.8, 59.0, 50.0, 34.0, 33.8, 32.0, 30.0, 29.95, 29.92, 29.9, 29.88, 29.85, 29.8, 29.7, 29.6, 29.4, 29.35, 24.8, 24.7, 22.7, 14.1. LRMS (MALDI-TOF, positive) m/z $[C_{434}H_{805}N_{21}O_{105} + Na]^+$ calc.: 8015.8 (0.61%) and 8020.8 (100%); found 8027.5 (100%).

Author contributions

J. E. synthesized all compounds and composite materials used for this study and completed impedance measurements. J. E., T. C. S. and A. C. analyzed the impedance experiments. C. O. Z.-P. and V. E. W. completed all POM, DSC and XRD experiments. D. S. completed all solid-state NMR experiments. C. O. Z.-P., V. E. W. and J. E. performed XRD, POM, and DSC experiments and their analysis. D. S. and V. K. M. performed solid state NMR investigation. J. E., C. O. Z.-P. and D. S. wrote the first draft of manuscript; all authors participated in the revisions of the manuscript and C.-C. L. and V. E. W. finalized the manuscript. C. C. L., V. E. W., and V. K. M. acquired funding. C.-C. L. conceived and designed the project.

Conflicts of interest

There are no conflicts to declare.

Data availability

The data supporting this article have been included as part of the supplementary information (SI). Supplementary information: NMR spectra of synthesized compounds, DSC, POM, XRD and impedance data (file type, PDF). See DOI: https://doi.org/10.1039/d5tc04203h.

Acknowledgements

We are grateful to Dr Ping Zhang of the Department of Chemistry, University of Calgary, for recording all the ESI HRMS spectra. This study was funded by operating grants from the Natural Sciences and Engineering Research Council of Canada (NSERC) to C.-C. L. (RGPIN-2024-04267) and V. E. W. (RGPIN-2022-03548). J. E., A. C., T. C. S. and C.-C. L. thank the University of Calgary for the support of the current project. The Chemistry Centre Magnetic Resonance (C^2MR) Facility for Solids is supported by the Canada Foundation for Innovation (CFI), Government of Alberta, and the University of Alberta.

Notes and references

1 C. S. Bonnet, P. H. Fries, A. Gadelle, S. Gambarelli and P. Delangle, *J. Am. Chem. Soc.*, 2008, **130**, 10401–10413.
2 E. Bilensoy and A. A. Hincal, *Expert Opin. Drug Delivery*, 2009, **6**, 1161–1173.
3 G. Varan, C. Varan, N. Erdoğar, A. A. Hıncal and E. Bilensoy, *Int. J. Pharm.*, 2017, **531**, 457–469.
4 J. Li and X. Loh, *Adv. Drug Delivery Rev.*, 2008, **60**, 1000–1017.
5 Á. Martínez, C. O. Mellet and J. M. G. Fernández, *Chem. Soc. Rev.*, 2013, **42**, 4746–4773.
6 C. Bienvenu, Á. Martínez, J. L. J. Blanco, C. D. Giorgio, P. Vierling, C. O. Mellet, J. Defaye and J. M. G. Fernández, *Org. Biomol. Chem.*, 2012, **10**, 5570–5581.
7 F. Sallas and R. Darcy, *Eur. J. Org. Chem.*, 2008, 957–969.
8 M. Votava and B. J. Ravoo, *Chem. Soc. Rev.*, 2021, **50**, 10009–10024.
9 P.-L. Champagne, R. Kumar and C.-C. Ling, in *Cyclodextrin Applications in Medicine, Food, Environment and Liquid Crystals*, ed. S. Fourmentin, G. Crini and E. Lichtfouse, Springer International Publishing, Cham, 2018, pp. 183–240.
10 C.-C. Ling, R. Darcy and W. Risse, *J. Chem. Soc., Chem. Commun.*, 1993, 438–440.

11 P.-L. Champagne, D. Ester, S. Ward, V. E. Williams and C.-C. Ling, *ChemPlusChem*, 2017, **82**, 423–432.
12 P.-L. Champagne, D. Ester, M. Zeeman, C. Zellman, V. E. Williams and C.-C. Ling, *J. Mater. Chem. C*, 2017, **5**, 9247–9254.
13 S. Ward, O. Calderon, P. Zhang, M. Sobchuk, S. N. Keller, V. E. Williams and C.-C. Ling, *J. Mater. Chem. C*, 2014, **2**, 4928–4936.
14 L. Chen, T.-H. Hu, H.-L. Xie and H.-L. Zhang, *J. Polym. Sci., Part A: Polym. Chem.*, 2010, **48**, 2838–2845.
15 F. Yang, Y. Zhang and H. Guo, *New J. Chem.*, 2013, **37**, 2275.
16 P.-L. Champagne, D. Ester, A. Bhattacharya, K. Hofstetter, C. Zellman, S. Bag, H. Yu, S. Trudel, V. K. Michaelis, V. E. Williams, V. Thangadurai and C.-C. Ling, *J. Mater. Chem. A*, 2019, **7**, 12201–12213.
17 A. Che, C. O. Zellman, D. Sarkar, S. Trudel-Lachance, J. Espejo, V. K. Michaelis, V. E. Williams and C.-C. Ling, *J. Mater. Chem. C*, 2023, **11**, 4153–4163.
18 A. Che, C. O. Zellmann-Parrotta, D. Sarkar, J. Espejo, V. K. Michaelis, T. C. Sutherland, V. E. Williams and C.-C. Ling, *Carbohydr. Polym.*, 2025, **359**, 123587.
19 J. Espejo, C. O. Zellmann-Parrotta, D. Sarkar, A. Che, V. K. Michaelis, V. E. Williams and C.-C. Ling, *Chem. – Eur. J.*, 2024, **30**, e202403232.
20 P.-L. Champagne, D. Ester, D. Polan, V. E. Williams, V. Thangadurai and C.-C. Ling, *J. Am. Chem. Soc.*, 2019, **141**, 9217–9224.
21 Y. Mai and A. Eisenberg, *Chem. Soc. Rev.*, 2012, **41**, 5969.
22 C. Li, Q. Li, Y. V. Kaneti, D. Hou, Y. Yamauchi and Y. Mai, *Chem. Soc. Rev.*, 2020, **49**, 4681–4736.
23 H. Minamikawa, T. Murakami and M. Hato, *Chem. Phys. Lipids*, 1994, **72**, 111–118.
24 H. Parrot-Lopez, C. C. Ling, P. Zhang, A. Baszkin, G. Albrecht, C. De Rango and A. W. Coleman, *J. Am. Chem. Soc.*, 1992, **114**, 5479–5480.
25 L. J. López-Méndez, E. E. Cuéllar-Ramírez, N. C. Cabrera-Quiñones, Y. Rojas-Aguirre and P. Guadarrama, *Int. J. Biol. Macromol.*, 2020, **164**, 1704–1714.
26 C. Fong, T. Le and C. J. Drummond, *Chem. Soc. Rev.*, 2012, **41**, 1297–1322.
27 Y. Zou, X. Zhou, J. Ma, X. Yang and Y. Deng, *Chem. Soc. Rev.*, 2020, **49**, 1173–1208.
28 D. W. Krevelen and K. te Nijenhuis, *Properties of polymers: their correlation with chemical structure their numerical estimation and prediction from additive group contributions*, Elsevier, Amsterdam, 4th completely rev. ed edn, 2009.
29 A. Che, C. O. Zellman, D. Sarkar, S. Trudel-Lachance, J. Espejo, V. K. Michaelis, V. E. Williams and C.-C. Ling, *J. Mater. Chem. C*, 2023, **11**, 4153–4163.
30 F. Neese, *WIREs Comput. Mol. Sci.*, 2022, **12**, e1606.
31 A. M. Squires, R. H. Templer, J. M. Seddon, J. Woenckhaus, R. Winter, S. Finet and N. Theyencheri, *Langmuir*, 2002, **18**, 7384–7392.
32 H. Guo, J. H. Jeong and J.-C. Kim, *Colloids Surf., A*, 2016, **495**, 1–10.
33 T. H. Do, H.-J. Kim, M. L. Nguyen and B.-K. Cho, *Crystals*, 2020, **10**, 193.
34 J.-W. Choi and B.-K. Cho, *Soft Matter*, 2011, **7**, 4045.
35 M. Wilkening and P. Heitjans, *Chem. Phys. Chem.*, 2012, **13**, 53–65.
36 S. Barcellona, S. Colnago, L. Codecasa and L. Piegari, *J. Energy Storage*, 2023, **73**, 109202.
37 F. Bloch, *Phys. Rev.*, 1946, **70**, 460.
38 A. Pines, M. G. Gibby and J. S. Waugh, *J. Chem. Phys.*, 2003, **56**, 1776.
39 S. R. Hartmann and E. L. Hahn, *Phys. Rev.*, 1962, **128**, 2042.
40 G. M. Bernard, A. Goyal, M. Miskolzie, R. McKay, Q. Wu, R. E. Wasylishen and V. K. Michaelis, *J. Magn. Reson.*, 2017, **283**, 14–21.